Materials Today Advances 19 (2023) 100414

Contents lists available at ScienceDirect

Materials Today Advances

journal homepage: www.journals.elsevier.com/materials-today-advances/

Generating colours through a novel approach based on spatial ALD and laser processing

A. Frechilla [a,b], A. Sekkat [b], M. Dibenedetto [b], F. lo Presti [b,c], L. Porta-Velilla [a], E. Martínez [a], G.F. de La Fuente [a], L.A. Angurel [a,**], D. Muñoz-Rojas [b,*]

[a] Instituto de Nanociencia y Materiales de Aragón, CSIC-Universidad de Zaragoza, María de Luna 3, E-50018, Zaragoza, Spain
[b] Univ. Grenoble Alpes, CNRS, Grenoble INP, LMGP, F-38000, Grenoble, France
[c] Dipartimento di Scienze Chimiche, Università di Catania, V. le Andrea Doria 6, I-95125, Catania, Italy

ARTICLE INFO

Keywords:
LIPSS
SALD
Iridescence
Interference colours
Laser

ABSTRACT

This work studies the combination of direct femtosecond laser structuring of metal surfaces and Spatial Atomic Layer Deposition (SALD) of metal oxides as a novel approach to generate colours on different types of day-to-day metallic objects. In particular, a stainless-steel knife and an outdated 25 ct Dutch florin coin have been selected for the study. Our results show that it is possible both, to preserve the iridescence properties produced by laser processing and to tune the final metal surface colour by controlling the thickness of the ZnO coating. At the same time, this oxide coating could act as a protecting layer for the original material. We thus explore two different strategies to generate colour, namely, iridescence and interference, which can be even developed selectively. This novel methodology to colour metallic surfaces is a promising route to achieve cheap, scalable, and high-throughput processing methods and opens up a new avenue of possibilities and applications related to colour.

1. Introduction

Colours are essential to humanity in their visual perception of the world, serving as media, as a symbol, or as adornment. It is difficult to mention a branch of human activity in which colour would not occupy a significant position, either from an artistic-aesthetic point of view, or from the psychophysiological perception and reaction to colour [1]. Therefore, one of the main interests of materials science and engineering is to generate more accurate colours using structural and functional coloured materials, even with the development of modern and more sustainable techniques.

Nature has three main sources of generating colours: pigments, structural colours, and bioluminescence. In case of structural colours, the colour is produced by micro- or nano-structures, as a result of different physical phenomena related to film interference, diffraction grating, scattering and photonic crystals [2]. In addition, these processes involved in structural colouration can be a promising route to obtain brilliant and dazzling colours, for decoration purposes, adaptive camouflage, or label marking, among others.

Several fabrication methods can be used to generate a structural colour. These include, for instance, electron beam lithography [3,4], two-photon polymerization lithography [5], ion beam lithography [6,7], ion milling [8] or nanoimprint lithography [9,10]. However, these methods exhibit a slow fabrication rate, require highly precise and costly equipment, and, as a consequence, the working surfaces are limited. Therefore, they are not suitable for the large-scale production of cost effective coloured surfaces [11].

Lasers have been used to generate coloured surfaces using two different physical processes. In the first one, by controlling the thickness of an oxide layer on top of the metallic surface [12,13]. In the second one, by generating a nanostructure that behaves as a diffraction grating on the metallic surface [14,15]. The generation of Laser Induced Periodic Surface Structures (LIPSS) has emerged as a mask-free, flexible, versatile, and cheap contactless approach to modify surface properties. Furthermore, this colour-production method provides additional inherent advantages to laser processing. These include environmentally

* Corresponding author.
** Corresponding author.
E-mail addresses: afrechi@unizar.es (A. Frechilla), abderrahime.sekkat@grenoble-inp.fr (A. Sekkat), francesca.lopresti@phd.unict.it (F. lo Presti), porveli@unizar.es (L. Porta-Velilla), elenamar@unizar.es (E. Martínez), german.delafuente.leis@csic.es (G.F. de La Fuente), angurel@unizar.es (L.A. Angurel), david.munoz-rojas@grenoble-inp.fr (D. Muñoz-Rojas).

https://doi.org/10.1016/j.mtadv.2023.100414
Received 31 December 2022; Received in revised form 3 June 2023; Accepted 2 August 2023
Available online 18 August 2023

respectful methodology and the capability of modifying complicated shapes with a simple single-step process [12,16]. The most characteristic feature of LIPSS is that they behave as diffraction gratings, causing the surface to exhibit different colours at different viewing angles (angle--dependent), a phenomenon called iridescence. As the colouration effect depends on the angle of illumination and observation, the orientation of the ripple pattern relative to these angles and the LIPSS period are the dominant parameters [11,16–18].

According to a generally accepted theory, the spatial ripple period (Λ) is directly related to the laser wavelength (λ), so that, the structural patterns are normally equal to or smaller than λ [19–21]. The LIPSS structure period, which gives rise to these iridescence patterns, has been found to be related to the laser irradiation wavelength and the optical properties of the material. The relation between λ and Λ define two groups of nanostructures: Low-spatial frequency LIPSS (LSFL) with $\Lambda > \lambda/2$ and high-spatial frequency LIPSS (HSFL) with $\Lambda < \lambda/2$. In metals, LSFL, usually called ripples, are mainly characterized by $\Lambda \sim \lambda$, and they are oriented near perpendicular to the beam polarization [22]. This offers the opportunity of generating different regions of the surface with different ripple geometries. As a consequence, when white light is irradiated from different directions on those nanostructured surfaces, different patterns can be selectively displayed [16,23].

LIPSS-based direct laser structuring can be used to generate colours on a wide variety of metals. These include, for example, gold, silver, copper, aluminium, steel and titanium [17,24]. Accordingly, colour can be induced in metal alloys commonly used in day-to-day objects and it can, therefore, exhibit a great potential for numerous industrial, commercial, and technical applications [16].

After laser processing, however, the surface of the material may become more reactive, leading to oxidation and/or other reactions that may degrade the irradiated surface in contact with ambient and reactive atmospheres [25,26]. As a consequence, the iridescent metal surfaces may need a protection coating [18]. Nevertheless, it is widely known that some metals are naturally resistant to corrosion as a result of nanometer-thick native oxide layer formation on their surface [27]. The latter could provide additional benefits and even new functionalities [28,29]. To begin with, the thin oxide layer can be used to tune the surface colour. In the case of ZnO for example, it also shows strong antibacterial activity against *E. coli* and *S. aureus* bacteria, good mechanical durability and enhanced anti-stain qualities [30]. It would be therefore convenient to deposit an oxide thin film such as a ZnO coating over the nanostructured metal surface. The film should be deposited with a fine control of the thickness and conformal enough so that the nanostructured surface morphology is maintained.

In this context, Atomic Layer Deposition (ALD) appears as an adequate technique to deposit such protective layers with thicknesses in the nanometer range and good conformality. ALD is a chemical gas-phase deposition technique that uniquely relies on the alternate pulsing of precursors, separated in time, that react with the surface in a self-limiting manner [31,32]. These characteristics result in the development of homogeneous ultra-thin coatings with atomic-scale control of material thickness and composition, even on non-planar substrates and complex features, for example, nanorods, nanowires, deep trenches, nanoparticles, and mesoporous and nanoporous surfaces [31,33]. However, ALD has a low deposition rate and is mostly performed in vacuum conditions. These represent drawbacks for the industrial application of ALD for low-cost, low-added value applications.

Recently, Spatial ALD (SALD) has emerged as an alternative ALD approach [34,35]. This novel technique is based on separating the precursors in space rather than in time [36]. As a result, there is no need for the typical ALD purge steps and deposition rates become up to a hundred times faster [37,38]. Additionally, the deposition using SALD can be easily performed at atmospheric pressure for several applications. Similar to ALD, highly conformal coatings with a fine thickness control can be obtained via SALD. Therefore, this process is more suitable to scale up and for industrial and commercial applications [39].

Furthermore, as stated above, the deposited SALD thin films can tune and modify the colour generated by the laser surface treatments, hence, create different colour schemes, and add new functionalities. In this case, the colour is generated by the interference effects due to the thickness of the deposited SALD coating and the passivation oxide layer formed after the laser treatment [18]. The SALD approach also offers the possibility of coating direct patterning [34], which could facilitate the generation of different colours in different regions. Finally, the spatial approach permits to have both ALD and CVD deposition conditions, thus giving an extra degree of freedom in tuning the coating properties [40].

In this work, we present the combination of LIPSS-based direct laser structuring and SALD to colour metallic surfaces. Two day-to-day objects are used as a proof of concept of the proposed method. These are an outdated 25 ct Dutch florin coin made of Nickel-Zinc alloy and a Stainless steel knife. These items provide two representative overused, non-planar surfaces from out-of-laboratory objects. This study constitutes a proof of concept that colour and iridescence can be combined in everyday objects for decoration purposes, such as to design a commemorative coin or customized knife.

2. Materials and methods

The items selected for this study were two different metallic objects that differ on the composition and surface characteristics: outdated coins (25 ct Dutch florin) made of nickel alloyed with zinc (97%at nickel and 3%at zinc) and a stainless steel knife. The colouring fabrication route employed in this work is represented in Fig. 1. In a first step, the selected object surfaces were treated using a femtosecond laser to generate a LIPSS nanostructure. In a second one, the resulting nanostructured surface was coated with ZnO using the SALD process.

A linearly polarized femtosecond laser (Carbide model from Light Conversion, Vilnius, Lithuania) equipped with a harmonic generator was used in this work. Its emission wavelength was selected at $\lambda = 515$ nm, its pulse duration at $\tau = 249$ fs, and its pulse repetition frequency at $f = 200$ kHz. The laser beam was moved by a galvanometer mirror system at a given speed, using a specific control software (DMC, Vilnius, Lithuania). The output laser beam exhibited a Gaussian energy profile, with a $1/e^2$ intensity decay dimension $2r = 50$ μm. Sample surfaces were treated using a laser beam scan configuration with the particular laser parameters detailed in Table 1. These proposed laser treatments were the result of an optimization process which included testing of several laser parameters. Logos of both research institutes (INMA and of LMGP) were initially marked on the knife blade, before the full blade surface was treated with the same processing parameters.

A home-made SALD system was used to deposit the oxide coatings [36,41]. The conditions for the SALD process were as follows: Diethylzinc precursor $(C_2H_5)_2Zn$ (DEZ) and water were used as ZnO precursors. The DEZ was bubbled using a nitrogen flow of 30 sccm while 150 sccm for H_2O, and respectively diluted in 270 and 300 sccm of N_2. Nitrogen was also used as inert gas barrier with a total flow rate of 900 sccm to separate the precursors. The temperature of the substrate was maintained at 200 °C. The distance between the substrate and the SALD injection manifold was approximately 150 μm with a scanning speed of 100 mm/s.

The surface microstructural characterization was performed in a FEG ZEISS Gemini 300 field-emission scanning electron microscope (SEM) (Carl Zeiss, Jena, Germany) equipped with an energy dispersive X-ray spectroscopy (EDX) system with a SDD detector (BRUKER AXS-30mm^2) operated at 10 kV. Additional characterization was performed with a field-emission scanning electron microscope (FESEM, MERLIN Carl Zeiss GmbH, Oberkochen, Germany) using secondary electron (SE), in-lens, and backscattered (ESB) detectors. The electron beam acceleration voltage was set to 5 kV. Surface topographic cross-sections were analysed by Scanning Transmission Electron Microscopy (STEM) and High Resolution Transmission Electron Microscopy (HRTEM) using a Tecnai F30 microscope (FEI Company, Hillsboro, OR, USA), also equipped with

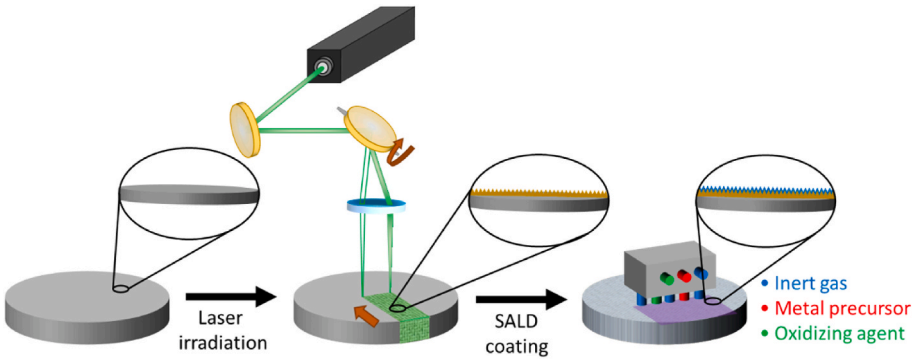

Fig. 1. Schematic description of the colouration process combining surface laser nanostructuring and SALD coating.

Table 1
Laser parameters applied on the different objects subjected to this study. The rest of the processing parameters were maintained in all treatments: $\lambda = 515$ nm; $\tau = 249$ fs; $f = 200$ kHz.

Object	Power [W]	Pulse energy [μJ]	Laser scan speed [mm/s]	Distance between lines [μm]
Knife blade INMA logo LMGP logo	1.32	6.6	2500	25
25 Dutch florin	8.71	43.5	2400	10

a high-angle annular dark field (HAADF) detector. Sample preparation was performed with a Focused Ion Beam (FIB) in a Dual Beam Helios 650 (FEI Company, Hillsboro, OR, USA) apparatus, using 30 kV Ga^+ ions for the initial steps and 5 kV for final thinning. Prior to the preparation of a FIB lamella, a protective C cap layer was deposited at the region of interest.

Atomic force microscopy (AFM) measurements were performed with a scanning probe microscope (SPM) Ntegra Aura system (NT-MDT, Moscow, Russia). The analysis of the AFM measurements was carried out using Gwyddion software (version 2.53).

Iridescence was measured with a home-made set-up based on the Bragg diffraction law [42], using a super-continuum laser (450–2400

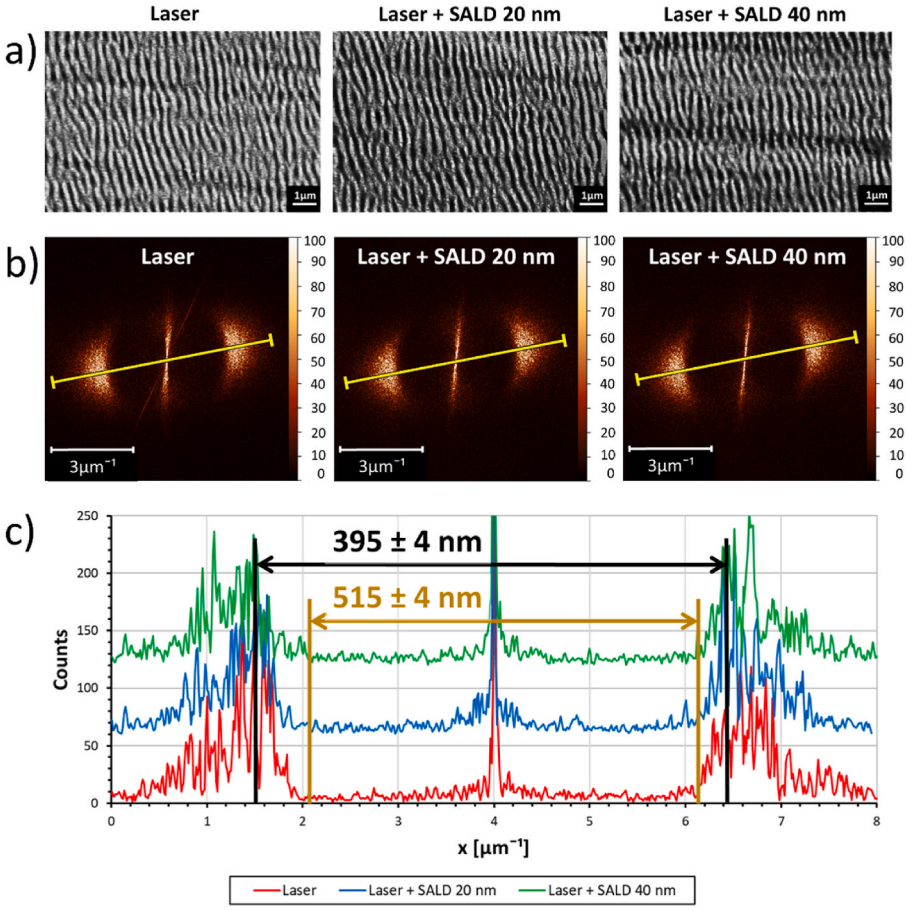

Fig. 2. (a) SEM micrograph of the knife surface before coating and after 20 nm and 40 nm of ZnO SALD coating. b) 2D fast Fourier transform images of SEM micrographs of the laser nanostructured knife surface with no coating, 20 nm and 40 nm-thick ZnO coatings. The SEM images that were selected to perform this analysis were taken with a magnification of 1 K and are shown in Figure A1 of Supplementary material. c) Corresponding profiles along the lines drawn in b).

nm) (SC500,FYLA, Valencia, Spain) as illumination source and a BLACK-Comet-SR-50 Miniature Spectrometer (StellarNet Inc, Tampa, USA). The diameter of the laser spot size was approximately 1 mm. The nanostructure can create a diffraction grid and this maximum is related to the period of the grid by Ref. [42]:

$$\sin\theta_o + \sin\theta_i = \lambda/\Lambda \quad (1)$$

where θ_o is the observation angle, θ_i the illumination angle, both measured from the normal to the sample surface, λ, the wavelength where the maximum appears and Λ the period of the diffraction grid.

3. Results and discussion

3.1. Modifications in the stainless-steel knife surface

A laser treatment covering the full blade was performed over the knife surface, using the laser processing parameters indicated in Table 1. The combination of laser nanostructuring with a Spatial ALD coating is the key part of this novel process. The following steps are thus aimed at understanding the effect of this thin film coating.

The analysis of the surface microstructure with electron microscopy confirms the low influence of the coating on the iridescence behaviour of the samples. SEM micrographs included in Fig. 2 (a) show that nanostructures are clearly observable in the three regions, even for the sample with a thicker ZnO coating. In addition, LIPSS morphology is very similar within the three surfaces. The LIPSS period, measured directly from the SEM images, is 390 ± 8 nm for the non-coated layer; 385 ± 14 nm for the 20 nm-thick coating and 392 ± 12 nm for the 40 nm-thick ZnO coating. These values correspond to approximately 0.75 times the laser output wavelength (515 nm). This is in agreement with previous reports, where the LSFL spatial period is found between λ and λ/2 [19–21] for these materials.

The 2D Fast Fourier transform (2D-FFT) of the SEM images allows us to determine the LIPSS period of larger surfaces (about 6000 μm^2). Fig. 2 (b) shows the 2D-FFT images obtained on the three surfaces. The maps presented in Fig. 2 show that the generated nanostructures are similar in the three samples, approaching a LIPPS period of 395 ± 4 nm. In addition, these analyses provide us with more complementary information about LIPSS. We can barely spot a tilted line in Fig. 2(b) within the 2D-FFT corresponding to the laser processed sample. This is assigned to the presence of scratches and notches on the knife's surface, already present before the laser treatment as a result of its common use. An important observation is the presence of a "circular exclusion area" of about 515 ± 4 nm, which may indicate that the formation of LIPSS with a larger period than the laser incident wavelength has not occurred.

The proper deposition of the thin film using SALD has been confirmed by EDX. The measured compositions are presented in Table 2 and the clear increase in Zn content confirms the growth of the ZnO thin film.

These microstructural observations are confirmed by AFM measurements. Fig. 3 shows the AFM images and the profiles measured in the surface after the laser treatment and after coating with a 40 nm thick ZnO layer. These measurements provide additional information about the ripple depths and the gap distance (defined as the free space between ripples at half height). After the SALD deposition there are still well-defined ripples on the surface. At least two different ripples height values can be spotted on both surfaces. For the laser treated sample without coating, ripples heights of 43 ± 11 nm and 79 ± 10 nm can be observed. Similarly, for the 40 nm-thick ZnO coated sample, ripples with average heights of 37 ± 16 nm and 74 ± 7 nm were obtained, depending on the zone selected. These differences could be due to the above mentioned irregularities on the treated surfaces, which lack perfect flatness and homogeneity within the laboratory-type samples, adding difficulty to the AFM experiments.

Table 2
EDS quantification summary in atomic percentage (%at).

	Oxygen	Silicon	Chromium	Iron	Zinc
0 nm	2,67	2,10	13,55	81,68	0,00
20 nm	3,52	1,90	12,43	79,25	2,90
40 nm	3,95	1,80	13,03	77,17	4,05

The ripples period has also been estimated from AFM measurements, being similar in both samples, 400 ± 12 nm for the initial laser treated surface (Fig. 3 (a)) and about 407 ± 14 nm (Fig. 3 (b)) for the 40 nm-thick ZnO coated surface, in good agreement with the electron microscopy results. The empty space at half height between two undulations, or gap distances (for the laser treated sample: 225 ± 13 nm; for the 40 nm ZnO coated sample: 213 ± 17 nm) are consistent with the previous experiments.

Further analysis of the LIPSS cross-section structure was performed with TEM on the sample coated with the highest amount of ZnO. Images presented in Fig. 4 show that the ZnO coating covers completely the metallic surface, and is conformal enough to replicate the ripple structure. While the ripple height obtained from these cross-section images appear of the same order than those estimated from AFM experiments, they are slightly higher. Thus, the LIPSS height is about 102 ± 9 nm for bare ripples (i.e. non-coated) and decreases to 78 ± 7 nm, after SALD coating (40 nm-thick). The differences between both type of measurements could be due to the AFM resolution and tip size, but very likely denote some inhomogeneities on the treated surfaces, since the TEM lamella provides information of tiny specific area of the samples and, the AFM has shown that different areas with different LIPSS heights are present on the samples.

These nanostructures produce strong iridescence effects. The LMGP and INMA laboratory logos were initially generated in the steel surface using the fs laser treatment presented in Table 1. The generated surface effect exhibits an iridescence effect, as observed in Fig. 5(a), where iridescent greenish and bluish colours are observed from an angle of 40°. This suggests that this laser treatment can be employed for decorative purposes.

Moreover, Fig. 5 (b) shows some photographs that were taken at four different observation angles, selected to show the iridescence effect generated on the laser treated surface. The obtained iridescence colours are observed to change from blueish at low angles (20°) to yellowish at high angles (60°). Even after this second treatment, the logos continue to be visible on the knife's surface.

The observed iridescence effects can be explained using Equation (1) and the period of the diffraction grid determined in the previous analysis. Fig. 5 (c) shows the evolution of the expected iridescence colours for different observation and illumination angles. The measured colours are similar to those expected for an illumination angle of 50°. The positions of the four images presented in Fig. 5 (b) have been levelled as A, B, C and D.

Fig. 6 shows the iridescence of the surface after applying two ZnO SALD coatings, with approximate respective thicknesses of 20 nm and 40 nm. The first outcome that can be directly noticed in Fig. 6 (a) is that the induced changes in the optical response of the surface do not appear to be so significant. In consequence, the observed colours are similar in the three regions under different illumination and observation angles, as deduced from Fig. 6 b-d.

The changes in the iridescence related to the coating has been studied to determine the influence of the ZnO SALD thin film on light diffraction phenomena. The iridescence spectra of the samples with the different coatings are shown in Fig. 7. The optical response of the sample surface was recorded using an illumination angle of $\theta_o = 60°$ with respect to the normal and an observation angle of $\theta_i = 35°$. In all cases, they show a well-defined peak with a maximum at 547 nm. Applying Equation (1), a value of $\Lambda = 385$ nm is obtained, analogous to the LIPPS periods measured with other characterization techniques that have been reported. These measurements confirm that the surface nanostructures exhibit similar periods within the three surfaces studied.

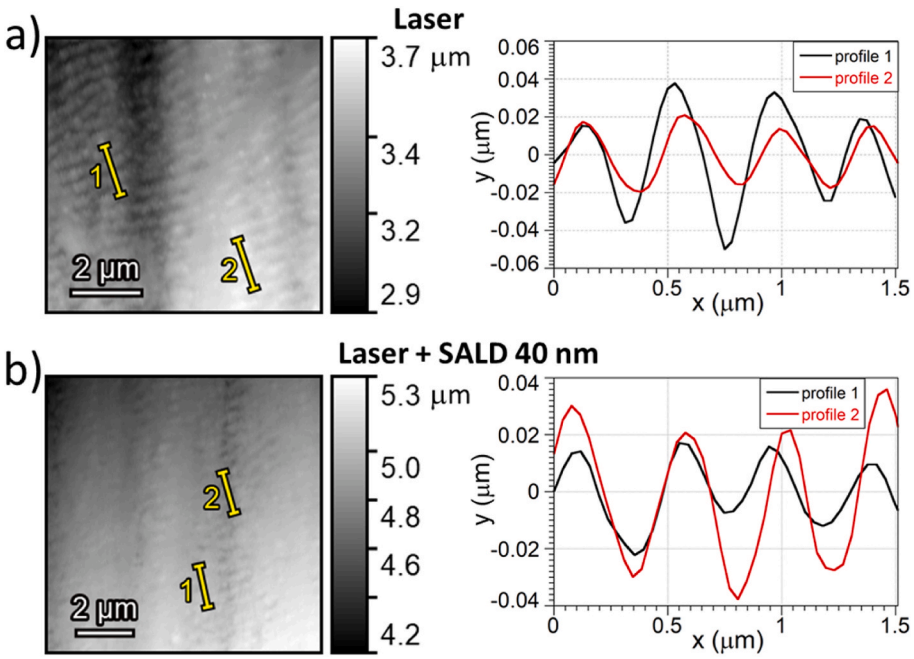

Fig. 3. AFM images and corresponding profiles of the stainless-steel knife surface: a) No coating, after laser treatment; b) After the 40 nm ZnO SALD coating. The background has been subtracted in the profiles presented.

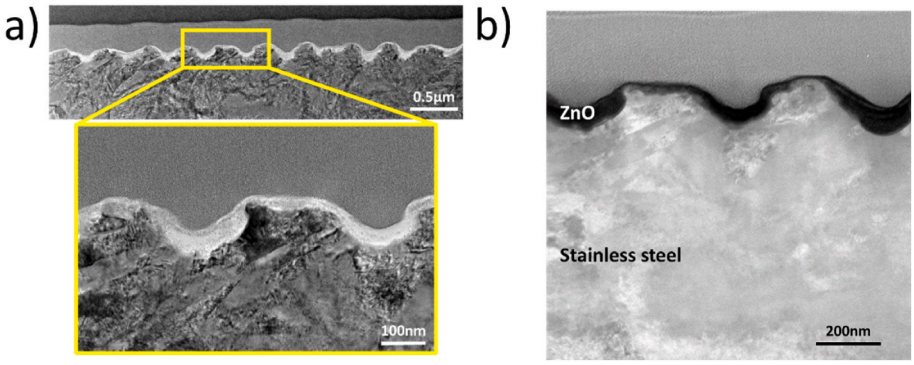

Fig. 4. Cross section of the stainless-steel knife LIPSS with theoretical 40 nm of ZnO SALD coating: a) HR-TEM image; b) STEM image.

The laser induces the LIPSS nanostructure that is responsible for the significant increase in the iridescence of the sample (visually perceptible in Fig. 6, when we compare the first photograph and the other three). The coating can affect the intensity of this generated iridescence. The thinnest ZnO coating (20 nm) maintains the original iridescence of the nanostructure. Conversely, the 40 nm-thick coating decreases the iridescence by ca. 23% with respect to the original laser treated surface. Such a decrease can be caused by some parasitic absorption at the ZnO coating [43]. Nevertheless, the iridescence in the 40 nm ZnO coating is still strong and visible.

These results confirm the deposition of the ZnO thin film without generating an evident change in colour. Therefore, it can be stated that below a threshold coating thickness, no colouring due to the interference phenomena appears. In fact, this particular case can be decisive in the case of using the ZnO thin film as a protective layer for the LIPSS-structured stainless-steel knife where, in some cases, the iridescence colour is sufficient and a coloured coating is not required.

3.2. Modifications in the 25 ct Dutch florin coin surface

The 25 ct Dutch florin coin provides a genuinely inhomogeneous surface, on the one hand, due to its inherent use as a coin, and, on the other hand, because several motifs with different heights are present in the patterns on the coin surface. In addition, the coin has been used to explore the changes induced by applying thicker ZnO SALD coatings.

Fig. 8 shows the final aspect of the Ni–Zn coin. Initially the laser treatment was applied to the full surface with the laser parameters indicated in Table 1. Three different SALD processes were subsequently applied in three quadrants of the coin with the aid of adequate masks. This front view of the coin shows that the ZnO thin film changes the colour of the original laser-treated coin. This change of colour is the result of the interference effects caused by the layer deposited on the metallic surface. This interference colour appears blue in the case of the coating with the lower thickness. It appears light purple and, subsequently, silver metallic grey in the two thicker ZnO coatings. The slight variations in colour within each particular quarter coated with ZnO are due to thickness gradients obtained during the deposition and which are difficult to avoid with the SALD deposition system employed, designed for larger, flat samples.

The thicknesses of the different coatings were measured by TEM analysis of the cross-section in lamellas obtained in each of the three coated regions. Fig. 9 shows the STEM images for the three ZnO coatings. The main outcome that can be determined from the micrographs is that the coating is extremely conformal in this case, reproducing

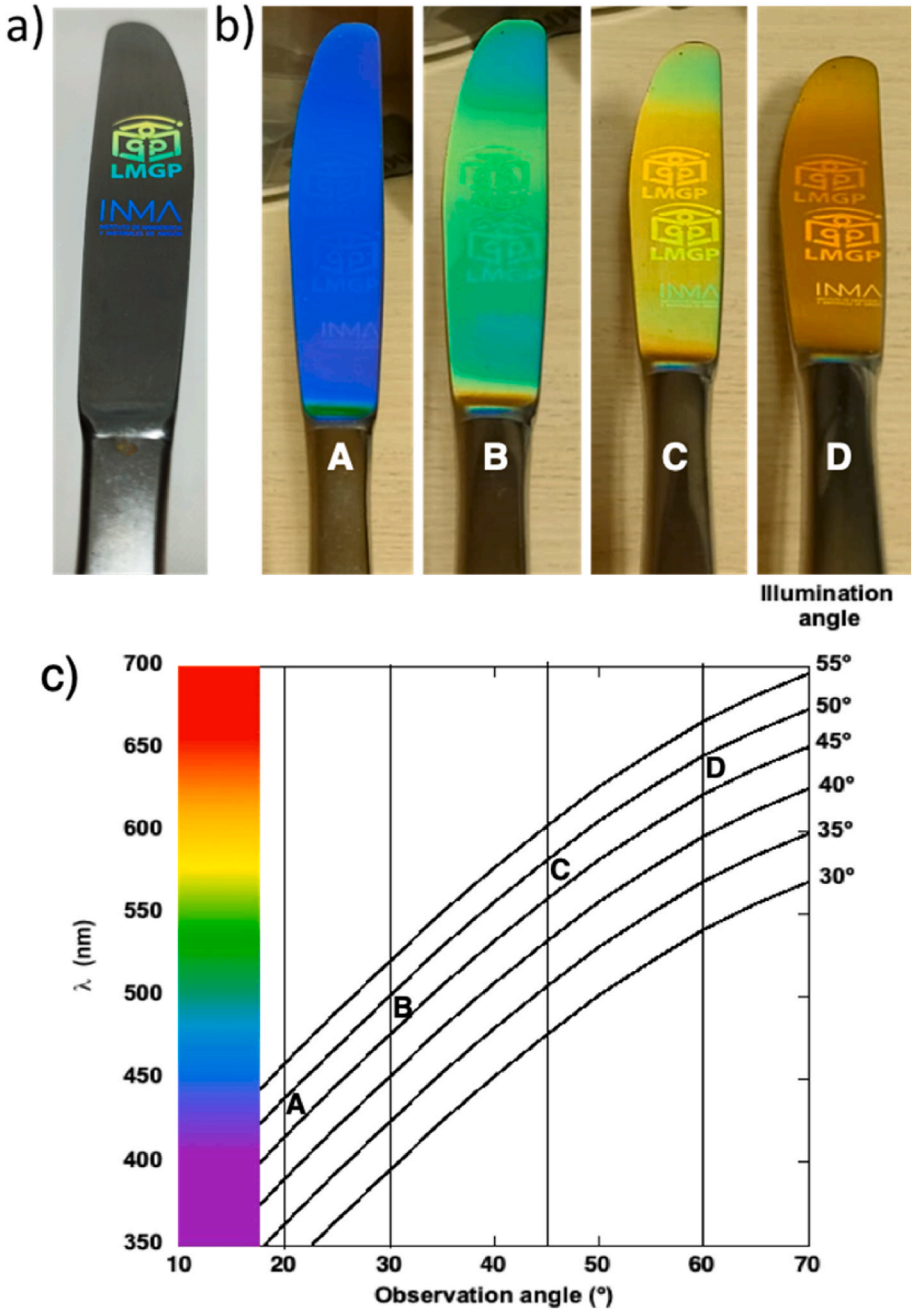

Fig. 5. Photographs of a representative laser treated stainless-steel knife: a) Surface after printing the LMGP and INMA logos, under an observation angle of 40°. b) Aspect of an equivalent knife surface after laser processing at different observation angles (20°, 30°, 45° and 60°, from left to right). (c) Theoretical predictions of the iridescence colours for different observation and illumination angles. Positions A, B, C and D correspond to colours observed in Fig. 5 (b).

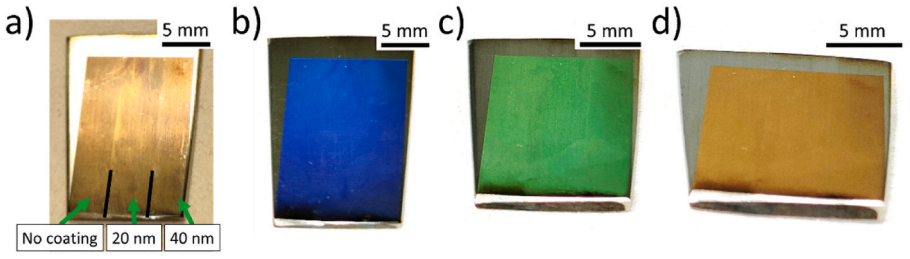

Fig. 6. a), b), c) and d): Normal image of the resultant colour of a knife blade after deposition of a ZnO thin film by SALD at different observation angles: a) front view, b) 20°, c) 50° and d) 70°.

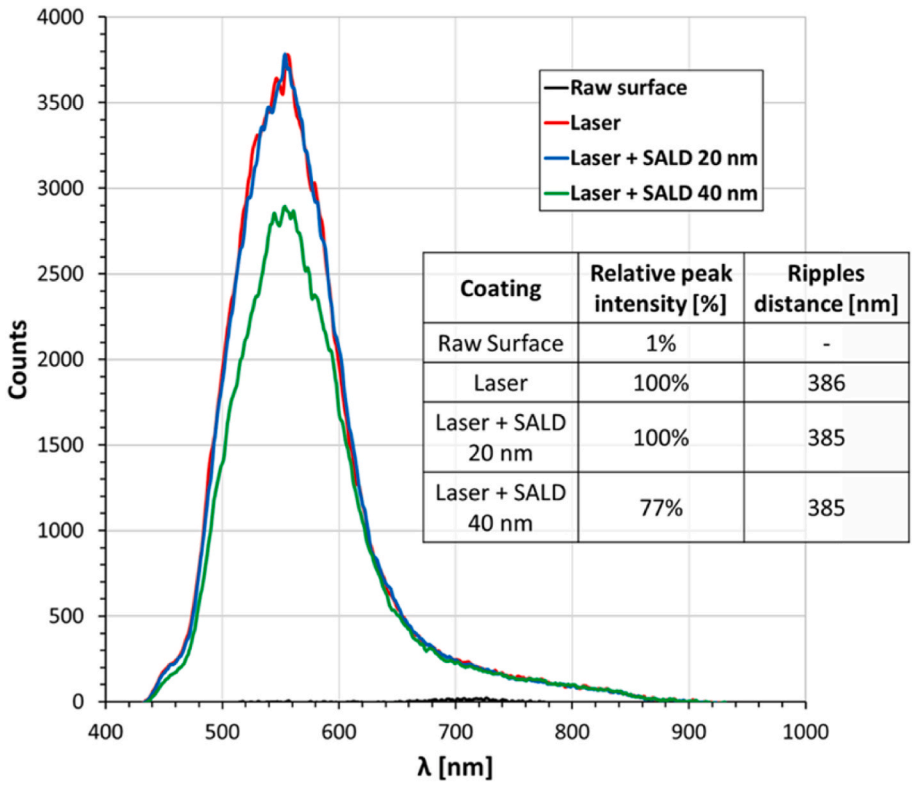

Coating	Relative peak intensity [%]	Ripples distance [nm]
Raw Surface	1%	-
Laser	100%	386
Laser + SALD 20 nm	100%	385
Laser + SALD 40 nm	77%	385

Fig. 7. Iridescence measurements observed on the three regions of the treated (laser + ZnO SALD coating) in the stainless-steel knife with an illumination angle of 60° and an observation angle of 35°. The relative peak intensity is calculated relative to the maximum intensity of the laser annealed. The raw surface is also plotted but it has almost 0 intensity.

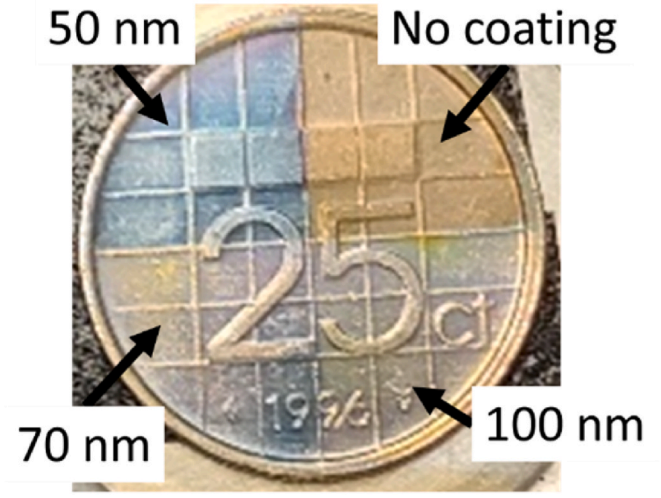

Fig. 8. Front view showing the resultant colour of the coin after laser processing and subsequent SALD of ZnO thin films with different thicknesses (No coating, 50 nm, 70 nm and 100 nm).

satisfactorily the LIPSS nanostructure. The estimated coating thicknesses are 50 ± 2 nm, 70 ± 4 nm and 100 ± 10 nm, respectively.

Taking into account this nanostructure, it is expected that the iridescence behaviour of the surface after laser irradiation is maintained after the SALD process. Fig. 10(a) shows the resultant iridescence colours at different observing angles (20°, 30°, 45° and 60°, from left to right) maintaining in all cases the same illumination angle. The iridescence is intense for all the ZnO coatings, producing some bright colours that are angle-dependent. In the selected observation angles, a dark blue, light blue, green and red colour can be observed. Furthermore, slight changes can be observed in the iridescence intensity for the different ZnO coatings. Fig. 10(b) shows the complete colour pattern generated by light diffraction that can be observed in the iridescence measurement apparatus. The full colour range is clearly observable in the wall behind the fibre detector. A similar behaviour was observed in the measurement of the four regions described above. It seems that the intensity of the iridescence light diffraction decreases when an interference colour is formed over the sample. The iridescence spectra were measured in order to confirm this statement. The particular iridescence spectra are presented in Fig. 10(c).

The above analysis becomes more complex for the coin, since its intricate topology, that is, the inscribed patterns and macro-defects, affect the measured iridescence patterns. Although the iridescence effect is perceived visually during the measurement, these defects cause light to be diffracted outside the detector, with their corresponding intensity changes in the measurement. In order to perform an accurate analysis, the intensity of each spectra has been scaled to the maximum intensity measured in the same position in a coin where only the laser treatment was performed. These measurements are presented in the supplementary material (Section S2). The decrease in intensity of around 20%, spotted for the laser treated surface, illustrates this measurement issues. This decrease is related to human error in sample positioning and to the intrinsic tolerance of the measurement apparatus.

As observed for the knife, the iridescence spectra measured in the coin surfaces exhibit a narrow and steep peak, even though the surface is not planar and has a complicated morphology, associated with the requirements of the coins. The latter observations suggest that both, the laser patterning and the SALD coating yield desirable control over surface quality. This is more evident when taking into account the spectra associated with the original raw surface, also included in Fig. 10(c) for comparison. In the four surfaces, the corresponding spectra show a well-defined peak with a maximum at 560 nm. In consequence, and applying

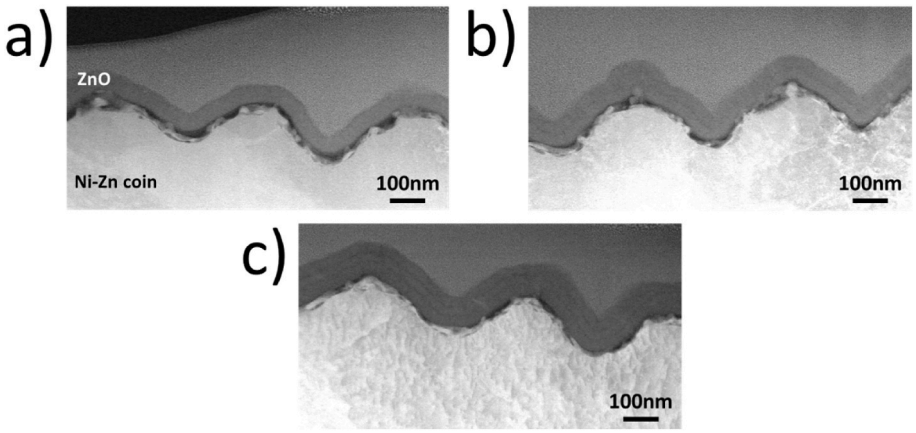

Fig. 9. STEM cross sections obtained on FIB-prepared lamellas of a LIPSS nanostructured Ni–Zn coin after SALD coating with different ZnO thickness: a) 50 nm; b) 70 nm; c) 100 nm.

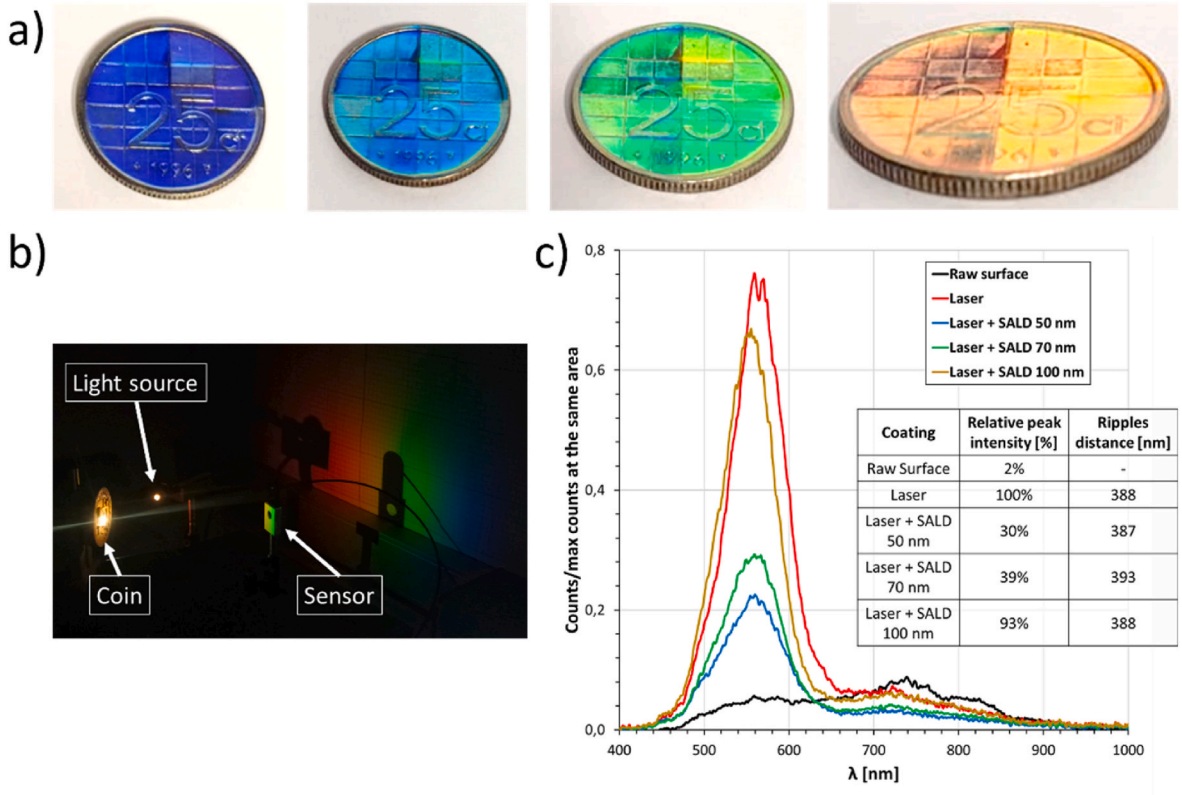

Coating	Relative peak intensity [%]	Ripples distance [nm]
Raw Surface	2%	-
Laser	100%	388
Laser + SALD 50 nm	30%	387
Laser + SALD 70 nm	39%	393
Laser + SALD 100 nm	93%	388

Fig. 10. a) Iridescence resultant colour in the coin at different observation angles: 20°, 30°, 45° and 60°, from left to right. b) Light diffraction observed in the iridescence measurement apparatus. c) Iridescence spectra measured in the three regions of the treated surface in the 25 ct coin with an illumination angle of 60° and an observation angle of 35°. The relative peak intensity is calculated relative to the maximum intensity measured on the laser treated surface. The spectrum obtained for the original raw surface is also plotted.

Equation (1), the generated LIPSS have a period of approximately, $\Lambda =$ 390 nm, also similar to the value obtained on the knife surface.

The iridescence intensity decreases when the LIPSS structure is coated. This visually observable decrease is estimated, in the case of thinner coatings, to be ca. 30% of the intensity observed on the original laser treated surface. However, a further increase in coating thickness produces a substantial rise in iridescence, almost achieving the original iridescence level for the thickest coating studied. Combining these results with those obtained for the knife, it appears that the iridescence level decreases when the ZnO coating thickness starts to increase and reaches values close to 50 nm. Above this value, it starts to increase again, recovering similar iridescence intensities for the thickest coatings reported here.

A possible explanation for the above observation could be related to the colour generating mechanism. The blue and purple colours are produced by interference of the light reflected in the two interfaces of the thin film coating. However, the ZnO layer is quasi-transparent, so that the light can diffract in the two interfaces, losing coherence and, therefore, intensity of the iridescence colour. Subsequently, the iridescence is almost recovered when increasing the thickness of the coating. A significant increase in the thickness of the thin film causes more light to be absorbed by the coating. Accordingly, the contribution of the lower

interface to the diffraction grating is nearly negligible and the initial iridescence intensity is recovered. In this case, the interference colour contribution is negligible and the now dominant natural metallic grey of the ZnO is observed.

These statements would imply that the coating is fully conformal to the LIPSS structure and that the laser nanostructures are translated to the surface of the samples with the additional SALD coating. SEM micrographs presented in Fig. 11 confirm this circumstance. Insets show a detail of the coating morphology where ZnO tiny crystals are observed to form a very dense structure over the LIPSS surface.

As for the knife, the 2D fast Fourier transforms of the SEM images of the coins allow us to determine the LIPSS period of larger surfaces. Fig. 12 shows the 2D-FFT images for the laser nanostructured samples for all the SALD ZnO coatings of the study obtained from the FESEM images presented in section S1 of the supplementary material.

The maps presented in Fig. 12 enable an estimate of the average LIPSS period, found around 402 ± 4 nm. Fig. 12 b) shows that the measured period is identical for all the coatings with the laser generated nanostructure. As the same laser has been used for processing the two items studied in this work, the period of the surface nanostructures is similar for the knife and the coin. Also analogous to the knife case, an "exclusion circular area" is observed at about 515 ± 4 nm where no LIPSS are formed, related to the laser irradiated wavelength.

4. Conclusions

This paper demonstrates that the generated LIPSS structure on a stainless steel knife can be successfully coated with a ZnO thin film deposited by SALD. The deposited coating barely affects the LIPSS period, determined as 395 ± 10 nm in all cases studied. In addition, there is no visual change in the color of the surface due to interference effects. On the contrary, the iridescence is changed by the coating, decreasing its intensity with increasing film thickness. Nevertheless, a 20 nm ZnO coating maintains the initial laser generated iridescence. This thin film coating is conformal and fully covers the surface, so it can be used as a protective thin film.

For the Ni–Zn coin studied, thicker ZnO coatings of 50–100 nm tune the colour of the coin as the result of the interference effects caused by the layer deposited on the metallic surface. Blue, purple and silver grey colours can be obtained respectively for 50, 70 and 100 nm ZnO coatings. The thin film coating changes the intensity of the laser generated iridescence. The latter decreases sharply when an interference colour is visualized. This phenomenon is produced due to the fact that the ZnO layer is quasi-transparent, so that the light can diffract in the two interfaces, losing coherence and, therefore, intensity of the iridescence colour. 30% of the intensity is maintained for 50 nm ZnO coatings and 39% for 70 nm ZnO coatings. This effect is mitigated for thicker films (i.e. 100 nm), where 93% of the initial iridescence intensity is recovered. In all cases, the mean LIPSS period remains at ca. 402 ± 4 nm. In this case, the coating is highly conformal, satisfactorily following the LIPSS nanostructure.

The results presented in this study show that SALD deposited ZnO coatings with different thicknesses conform to the contour of the substrate's laser-induced LIPSS nanostructure. This process can allow tuning of the final obtained colour, even in an area-selective fashion of regular day-to-day objects with out-of-laboratory non-planar surfaces, such as a stainless-steel knife or an outdated 25 ct Dutch florin coin.

The combination of LIPSS-based direct femtosecond laser nanostructuring and subsequent Spatial ALD surface coating is a promising route to achieve cheap, scalable, and high-throughput colouring of metallic objects, based on two different colour strategies —iridescence and interference. These were both explored in this paper using scalable processing methods and the presented results open a new avenue of possibilities and applications related to colour.

Credit author statement

A. Frechilla: Investigation, Visualization, Writing – original draft A. Sekkat, M. Dibenedetto, F. lo Presti, L. Porta-Velilla, E. Martínez: Investigation, Visualization, Writing – review & editing G. F. de La Fuente, L. A. Angurel, D. Muñoz-Rojas: Conceptualization, Methodology, Writing – review & editing, Visualization, Project administration, Funding acquisition.

Declaration of competing interest

The authors declare the following financial interests/personal relationships which may be considered as potential competing interests: David Munoz-Rojas reports financial support was provided by European Union. Alejandro Frechilla Zabal reports financial support was provided by Gobierno de Aragón. Francesca lo Presti reports financial support was provided by Government of Italy Ministry of Education University and Research.

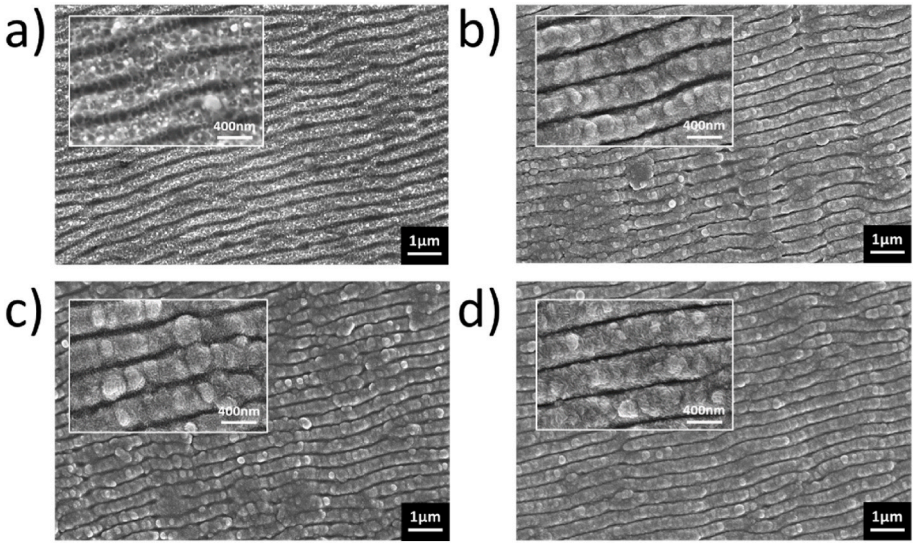

Fig. 11. SEM micrographs of the coin surfaces after laser processing and SALD of ZnO coating thin films: a) no coating; b) 50 nm; c) 70 nm; d) 100 nm. Insets show a detail of the original ripples surface and of the ZnO coatings morphologies.

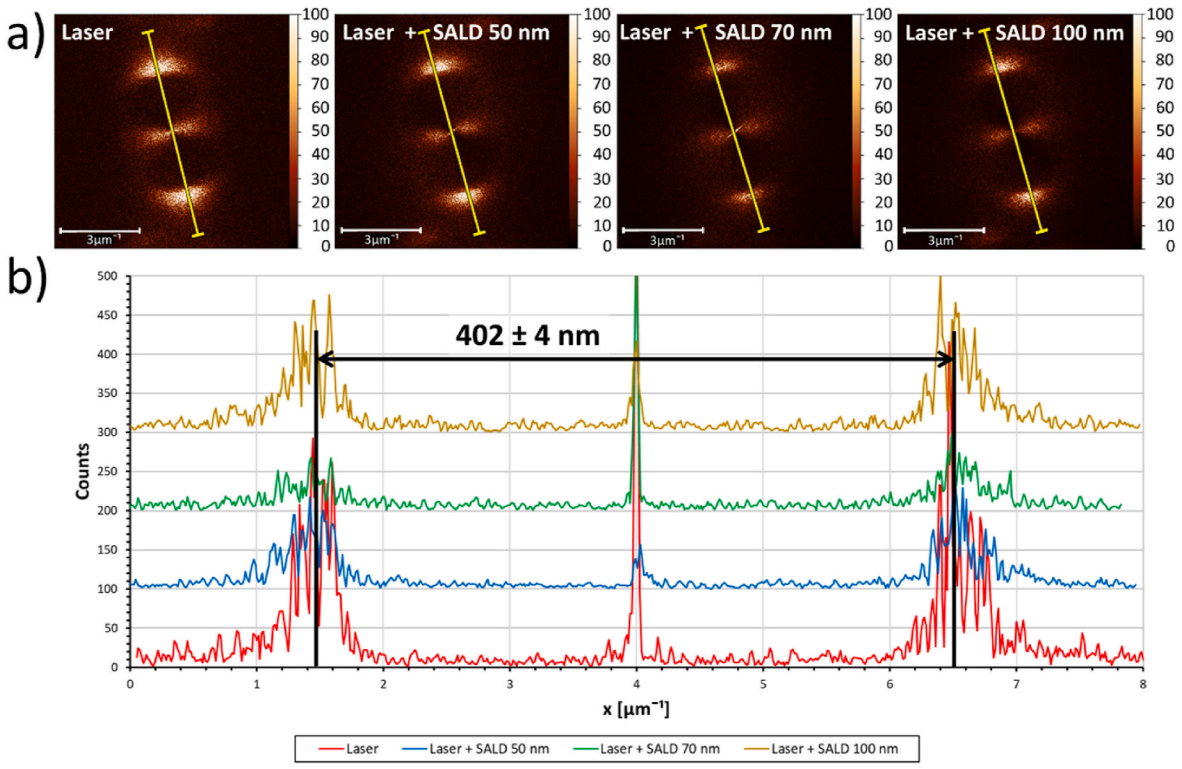

Fig. 12. a) 2D-FFT images of the SEM micrographs of the coin after laser processing with no coating, and 50 nm, 70 nm and 100 nm-thick SALD ZnO coatings (see SEM images in Figure A2 of the Supplementary material). b) Corresponding profiles obtained along the lines drawn in a).

Data availability

Data will be made available on request.

Acknowledgements

The authors gratefully acknowledge the financial support from EU project SPRINT (H2020-FETOPEN 801464), Spanish MCIN/AEI/10.13039/501100011033 (project PID2020-113034RB-I00) and from the Gobierno de Aragón (research group T54_23R). Authors also would like to acknowledge the use of Servicio General de Apoyo a la Investigación-SAI and Laboratorio de Microscopías Avanzadas at University of Zaragoza. A. Frechilla and L. Porta-Velilla acknowledge support of the Gobierno de Aragón through their predoctoral contract. DMR and FLP acknowledge support from the Ministère de l'Europe et des Affaires étrangères (MEAE) the Ministère de l'Enseignement Supérieur et de la Recherche (MESR) and the Ministero dell'Istruzione, dell'Università e della Ricerca (MIUR) through a PhC Galilée/Galileo project.

Appendix A. Supplementary data

Supplementary data to this article can be found online at https://doi.org/10.1016/j.mtadv.2023.100414.

References

[1] D.I. Nesterov, M.Y. Fedorova, Colour perception in ancient world, IOP Conf. Ser. Mater. Sci. Eng. 262 (2017), https://doi.org/10.1088/1757-899X/262/1/012139.
[2] J. Sun, B. Bhushan, J. Tong, Structural coloration in nature, RSC Adv. 3 (2013) 14862–14889, https://doi.org/10.1039/C3RA41096J.
[3] S. Daqiqeh Rezaei, J. Ho, T. Wang, J.K.W. Yang, S. Ramakrishna, Direct color printing with an electron beam, Nano Lett. 20 (2020) 4422–4429, https://doi.org/10.1021/acs.nanolett.0c01191.
[4] A.S. Roberts, A. Pors, O. Albrektsen, S.I. Bozhevolnyi, Subwavelength plasmonic color printing protected for ambient use, Nano Lett. 14 (2014) 783–787, https://doi.org/10.1021/nl404129n.
[5] J.Y.E. Chan, Q. Ruan, M. Jiang, H. Wang, H. Wang, W. Zhang, C.W. Qiu, J.K. W. Yang, High-resolution light field prints by nanoscale 3D printing, Nat. Commun. 12 (2021) 1–9, https://doi.org/10.1038/s41467-021-23964-6.
[6] B. Zeng, Y. Gao, F.J. Bartoli, Ultrathin nanostructured metals for highly transmissive plasmonic subtractive color filters, Sci. Rep. 3 (2013) 1–9, https://doi.org/10.1038/srep02840.
[7] F. Cheng, J. Gao, S.T. Luk, X. Yang, Structural color printing based on plasmonic metasurfaces of perfect light absorption, Sci. Rep. 5 (2015) 1–10, https://doi.org/10.1038/srep11045.
[8] F. Cheng, J. Gao, L. Stan, D. Rosenmann, D. Czaplewski, X. Yang, Aluminum plasmonic metamaterials for structural color printing, Opt. Express 23 (2015), 14552, https://doi.org/10.1364/oe.23.014552.
[9] M. Takeda, R. Takahara, N. Hasuike, Plasmonic color pixels fabricated by nanoimprint process, Opt. Rev. 27 (2020) 427–431, https://doi.org/10.1007/s10043-020-00610-y.
[10] S.H. Ahn, L.J. Guo, High-speed roll-to-roll nanoimprint lithography on flexible plastic substrates, Adv. Mater. 20 (2008) 2044–2049, https://doi.org/10.1002/adma.200702650.
[11] E.M. Garcell, S.C. Singh, H. Li, B. Wang, S.A. Jalil, C. Guo, Comparative study of femtosecond laser-induced structural colorization in water and air, Nanoscale Adv. 2 (2020) 2958–2967, https://doi.org/10.1039/c9na00804g.
[12] A.Y. Vorobyev, C. Guo, Colorizing metals with femtosecond laser pulses, Appl. Phys. Lett. 92 (2008) 1–4, https://doi.org/10.1063/1.2834902.
[13] E. Gaul, Coloring titanium and related metals by electrochemical oxidation, J. Chem. Educ. 70 (1993) 176–178, https://doi.org/10.1021/ed070p176.
[14] M. Soldera, F. Fortuna, S. Teutoburg-Weiss, S. Milles, K. Taretto, A.F. Lasag, Comparison of structural colors achieved by laser-induced periodic surface structures and direct laser interference patterning, J. Laser Micro Nanoeng. 15 (2020) 97–103, https://doi.org/10.2961/jlmn.2020.02.2004.
[15] J. Bonse, Quo vadis LIPSS?—recent and future trends on laser-induced periodic surface structures, Nanomaterials 10 (2020) 1–19, https://doi.org/10.3390/nano10101950.
[16] F.A. Müller, C. Kunz, S. Gräf, Bio-inspired functional surfaces based on laser-induced periodic surface structures, Materials 9 (2016), https://doi.org/10.3390/ma9060476.
[17] J. Bonse, S.V. Kirner, J. Krüger, Laser-induced periodic surface structures (LIPSS), Handb. Laser Micro- Nano-Eng. 23 (2021) 1–59, https://doi.org/10.1007/978-3-319-69537-2_17-2.
[18] J.M. Guay, A. Cala'Lesina, J.S. Baxter, P.G. Gordon, S.T. Barry, L. Ramunno, P. Berini, A. Weck, Coloring and Color Enhancement on Noble Metals Rendered by Plasmonic Effects via Multi-Burst Picosecond Pulses, Photonics North, PN 2017, 2017, https://doi.org/10.1109/PN.2017.8090580, 2017.
[19] J. Bonse, S. Gräf, Ten open questions about laser-induced periodic surface structures, Nanomaterials 11 (2021) 1–21, https://doi.org/10.3390/nano11123326.

[20] J.J.J. Nivas, S. Amoruso, Generation of supra-wavelength grooves in femtosecond laser surface structuring of silicon, Nanomaterials 11 (2021) 1–20, https://doi.org/10.3390/nano11010174.
[21] K.M. Tanvir Ahmmed, C. Grambow, A.M. Kietzig, Fabrication of micro/nano structures on metals by femtosecond laser micromachining, Micromachines 5 (2014) 1219–1253, https://doi.org/10.3390/mi5041219.
[22] J. Bonse, S. Gräf, Maxwell meets marangoni—a review of theories on laser-induced periodic surface structures, Laser Photon. Rev. 14 (2020) 1–25, https://doi.org/10.1002/lpor.202000215.
[23] J. Yao, C. Zhang, H. Liu, Q. Dai, L. Wu, S. Lan, A.V. Gopal, V.A. Trofimov, T. M. Lysak, Selective appearance of several laser-induced periodic surface structure patterns on a metal surface using structural colors produced by femtosecond laser pulses, Appl. Surf. Sci. 258 (2012) 7625–7632, https://doi.org/10.1016/j.apsusc.2012.04.105.
[24] J. Bonse, J. Krüger, S. Höhm, A. Rosenfeld, Femtosecond laser-induced periodic surface structures, J. Laser Appl. 24 (2012) 572–579, https://doi.org/10.2351/1.4712658.
[25] C. Florian, R. Wonneberger, A. Undisz, S.V. Kirner, K. Wasmuth, D. Spaltmann, J. Krüger, J. Bonse, Chemical effects during the formation of various types of femtosecond laser-generated surface structures on titanium alloy, Appl. Phys. Mater. Sci. Process 126 (2020) 1–11, https://doi.org/10.1007/s00339-020-3434-7.
[26] J. Bonse, A. Rosenfeld, J. Krüger, On the role of surface plasmon polaritons in the formation of laser-induced periodic surface structures upon irradiation of silicon by femtosecond-laser pulses, J. Appl. Phys. 106 (2009), 104910, https://doi.org/10.1063/1.3261734.
[27] Y. Yang, A. Kushima, W. Han, H. Xin, J. Li, Liquid-like, self-healing aluminum oxide during deformation at room temperature, Nano Lett. 18 (2018) 2492–2497, https://doi.org/10.1021/acs.nanolett.8b00068.
[28] H. Zhou, J. Li, S. Bao, J. Li, X. Liu, P. Jin, Use of ZnO as antireflective, protective, antibacterial, and biocompatible multifunction nanolayer of thermochromic VO2 nanofilm for intelligent windows, Appl. Surf. Sci. 363 (2016) 532–542, https://doi.org/10.1016/j.apsusc.2015.12.045.
[29] R.N. Jagtap, P.P. Patil, S.Z. Hassan, Effect of zinc oxide in combating corrosion in zinc-rich primer, Prog. Org. Coating 63 (2008) 389–394, https://doi.org/10.1016/j.porgcoat.2008.06.012.
[30] H.J. Choi, B.J. Park, J.H. Eom, M.J. Choi, S.G. Yoon, Achieving antifingerprinting and antibacterial effects in smart-phone panel applications using ZnO thin films without a protective layer, ACS Appl. Mater. Interfaces 8 (2016) 997–1003, https://doi.org/10.1021/acsami.5b11024.
[31] S.M. George, Atomic layer deposition: an overview, Chem. Rev. 110 (2010) 111–131, https://doi.org/10.1021/cr900056b.
[32] M. Leskelä, M. Ritala, Atomic layer deposition (ALD): from precursors to thin film structures, Thin Solid Films 409 (2002) 138–146, https://doi.org/10.1016/S0040-6090(02)00117-7.
[33] M. Knez, K. Nielsch, L. Niinistö, Synthesis and surface engineering of complex nanostructures by atomic layer deposition, Adv. Mater. 19 (2007) 3425–3438, https://doi.org/10.1002/adma.200700079.
[34] C.A.M. de la Huerta, V.H. Nguyen, A. Sekkat, C. Crivello, F. Toldra-Reig, P. B. Veiga, S. Quessada, C. Jimenez, D. Muñoz-Rojas, Gas-phase 3D printing of functional materials, Adv. Mater. Technol. 5 (2020), 2000657, https://doi.org/10.1002/admt.202000657.
[35] D. Muñoz-Rojas, J. Macmanus-Driscoll, Spatial atmospheric atomic layer deposition: a new laboratory and industrial tool for low-cost photovoltaics, Mater. Horiz. 1 (2014) 314–320, https://doi.org/10.1039/c3mh00136a.
[36] V.H. Nguyen, A. Sekkat, C. Jiménez, D. Muñoz, D. Bellet, D. Muñoz-Rojas, Impact of precursor exposure on process efficiency and film properties in spatial atomic layer deposition, Chem. Eng. J. 403 (2021), 126234, https://doi.org/10.1016/j.cej.2020.126234.
[37] D. Muñoz-Rojas, V.H. Nguyen, C. Masse de la Huerta, S. Aghazadehchors, C. Jiménez, D. Bellet, Spatial Atomic Layer Deposition (SALD), an emerging tool for energy materials. Application to new-generation photovoltaic devices and transparent conductive materials, Compt. Rendus Phys. 18 (2017) 391–400, https://doi.org/10.1016/j.crhy.2017.09.004.
[38] R.L.Z. Hoye, D. Muñoz-Rojas, S.F. Nelson, A. Illiberi, P. Poodt, F. Roozeboom, J. L. Macmanus-Driscoll, Research Update: atmospheric pressure spatial atomic layer deposition of ZnO thin films: reactors, doping, and devices, Apl. Mater. 3 (2015), https://doi.org/10.1063/1.4916525.
[39] D. Muñoz-Rojas, T. Maindron, A. Esteve, F. Piallat, J.C.S. Kools, J.M. Decams, Speeding up the unique assets of atomic layer deposition, Mater. Today Chem. 12 (2019) 96–120, https://doi.org/10.1016/j.mtchem.2018.11.013.
[40] K.P. Musselman, D. Muñoz-Rojas, R.L.Z. Hoye, H. Sun, S.L. Sahonta, E. Croft, M. L. Böhm, C. Ducati, J.L. MacManus-Driscoll, Rapid open-air deposition of uniform, nanoscale, functional coatings on nanorod arrays, Nanoscale Horizons 2 (2017) 110–117, https://doi.org/10.1039/c6nh00197a.
[41] V.H. Nguyen, J. Resende, C. Jiménez, J.-L. Deschanvres, P. Carroy, D. Muñoz, D. Bellet, D. Muñoz-Rojas, Deposition of ZnO based thin films by atmospheric pressure spatial atomic layer deposition for application in solar cells, J. Renew. Sustain. Energy 9 (2017), 21203, https://doi.org/10.1063/1.4979822.
[42] N. Bonod, J. Neauport, Diffraction gratings: from principles to applications in high-intensity lasers, Adv. Opt. Photonics 8 (2016) 156, https://doi.org/10.1364/aop.8.000156.
[43] A. Khan, V.H. Nguyen, D. Muñoz-Rojas, S. Aghazadehchors, C. Jiménez, N. D. Nguyen, D. Bellet, Stability enhancement of silver nanowire networks with conformal ZnO coatings deposited by atmospheric pressure spatial atomic layer deposition, ACS Appl. Mater. Interfaces 10 (2018) 19208–19217, https://doi.org/10.1021/acsami.8b03079.